JOURNAL OF GEOPHYSICAL RESEARCH, VOL. 111, E12006, doi:10.1029/2006JE002705, 2006

Radar properties as clues to relative ages of ridge belts and plains on Venus

George E. McGill[1] and Bruce A. Campbell[2]

Received 2 March 2006; revised 7 July 2006; accepted 13 July 2006; published 16 December 2006.

[1] An ongoing issue regarding the crustal evolution of Venus is whether or not certain features and processes occurred in the same sequence and at the same time globally. This paper seeks to test one aspect of "directional" models for the geologic history: the inference that all ridge belts are older than regional plains. This test involves traditional geologic analysis, but also involves the use of radar properties in a unique way. We use a simplified model for the ridge shape, and an estimate of the diffuse scattering behavior of the Venus surface, to determine the "true" backscatter coefficient of the slope of the ridge tilted away from the radar, and ratio this value to the echoes from nearby plains units. In general, ridge-forming terrain in these belts appears to have greater inferred backscatter coefficients, and thus decimeter-scale roughness, than the regional plains. Plains units closely adjacent to many ridge belts have higher backscatter than plains at some distance, which we infer is generally due to aeolian deposition of debris characterized by centimeter-scale microdunes or ripples where the belt topography interferes with wind patterns. The rougher apparent surface texture within the belt-forming terrain is not consistent with the gentle folding that forms the ridges, and so is likely a result of weathering or tectonic processes operating prior to belt deformation. We thus conclude that the material incorporated in the ridge belts we have studied predates the surrounding regional plains.

Citation: McGill, G. E., and B. A. Campbell (2006), Radar properties as clues to relative ages of ridge belts and plains on Venus, *J. Geophys. Res.*, *111*, E12006, doi:10.1029/2006JE002705.

1. Introduction

[2] An ongoing issue regarding the crustal evolution of Venus is whether or not certain features and processes occurred in the same sequence and at the same time globally. At one extreme is the view that there is a global stratigraphy [*Basilevsky and Head*, 1995, 1998, 2000], and thus a global synchronicity of processes and features. This model has been referred to as "directional" [*Guest and Stofan*, 1999]. In contrast to this is the "nondirectional model" [*Guest and Stofan*, 1999], which argues that if similar sequences do occur, they are not necessarily of the same age everywhere. This second view is similar to our understanding of Earth crustal evolution, where similar processes occur repeatedly (e.g., subduction and island arc formation). Venus is not the same as the Earth in some very important respects, including no liquid water and no plate tectonics during the preserved crustal record, so it is important to retain an open mind when considering the style of venusian tectonics.

[3] This paper seeks to test one element in the directional model; specifically, the inference that all ridge belts are older than regional plains. This test involves traditional geologic analysis, but also involves the use of radar properties in a unique way. Our results favor a preregional plains age for the ridge belts we have studied. The term "regional plains" refers to plains that are areally dominant on a regional (perhaps global) scale. Such plains are commonly mapped as "regional plains," or else as "plains with wrinkle ridges," a less desirable variant, by those preparing geological maps. In places, regional plains are directly in contact with ridges of ridge belts. Elsewhere, the plains close to ridge belts ("adjacent plains") differ in texture or backscatter from the regional plains. This difference could be due to a belt-related crustal unit distinct from regional plains, or to aeolian modification of the plains surface close to the ridge belts.

2. Relative Ages of Ridge Belts and Plains

[4] The relative ages of ridge belts and the surrounding plains are locally very clear from geologic relationships, but in other instances are ambiguous. The most robust examples of ridge belts older than regional plains occur where ridges are deformed by structures, such as grabens or radar-bright lineations, that are sharply truncated at contacts between these ridges and the regional plains. In other instances, ridges in ridge belts deform materials that are embayed by

[1]Department of Geosciences, University of Massachusetts, Amherst, Massachusetts, USA.
[2]Center for Earth and Planetary Studies, Smithsonian Institution, Washington, D. C., USA.

0148-0227/06/2006JE002705$09.00

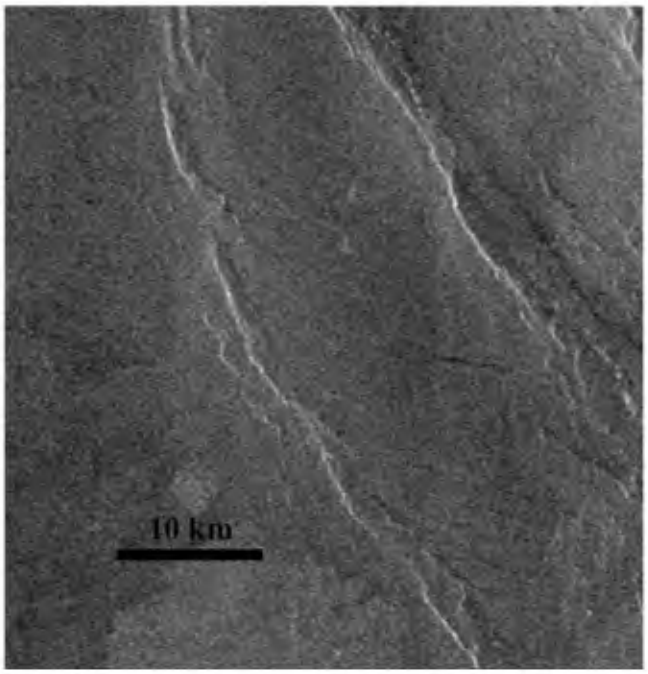

Figure 1. Ambiguous geologic age relationship, Laūma Dorsa. Ridges, Pandrosos Dorsa quadrangle. Ridges were mapped by *Rosenberg and McGill* [2001] as consisting of deformed plains materials, but the relationships also suggest that the ridges are embayed by the regional plains. Radar properties indicate that the ridges cannot be folded regional plains, but could be folded plains-like belt materials. North is up.

regional plains, a relationship that also strongly implies that the ridges are older than the regional plains. Excellent examples of both situations are found in Lavinia Planitia [*Squyres et al.*, 1992; *Ivanov and Head*, 2001].

[5] Commonly, however, there is not a clearly defined older material unit associated with a ridge belt, or else the belt involves a mappable older material for only part of its length. Where ridge belt ridges are partially or completely surrounded by regional plains, the common inference is that the plains embay the ridge belt (Figure 1). If the ridges of the belt are not cut by structures that terminate at contacts with plains, then this inferred embayment relationship may be in error. Without clear evidence for cross-cutting of structures, it is also possible that the ridge belts are comprised of deformed plains material (i.e., that the deformation postdates plains emplacement). The radar image contrast between ridges and plains does not necessarily imply a particular stratigraphic relationship, because the folding changes the local incidence angle, and hence the radar brightness, of the fold limbs. The radar-facing fold limb will have lower effective incidence angle and higher backscatter, while the far limb will have lower backscatter due to a higher effective incidence angle. This can result in a radar-image appearance that is indistinguishable from the commonly assumed embayment relationship. We use a simple model for radar scattering from a tilted surface to remove this geometric effect on the radar echoes from ridges, and to directly compare the scattering properties of fold limbs and adjacent plains.

3. Radar Scattering Model

[6] We use a simplified model for ridge geometry, and an estimate of the diffuse radar scattering behavior of the Venus surface, to estimate the "true" backscatter coefficient of the radar-dark "far" limb of a fold relative to the nearby plains material (Figure 2). Our assumptions are: (1) the fold limbs can be treated as planar for determining the average local incidence angle and effective scattering area, (2) diffuse scattering follows a $\cos^{1.5}$ dependence on local incidence angle [*Hagfors*, 1970], and (3) the folding process does not change the decimeter-scale morphology of the limb surface. Each of these assumptions will be discussed below, but taken together the corrected backscatter for a ridge far slope is

$$\sigma^o_{R-corrected} = \sigma^o_{R-observed} \frac{\sin(\phi+\alpha)}{\sin\phi} \left[\frac{\cos(\phi+\alpha)}{\cos\phi}\right]^{-1.5}, \quad (1)$$

where α is the slope angle of the ridge limb and ϕ represents the nominal incidence angle for a "locally flat" Venus. The

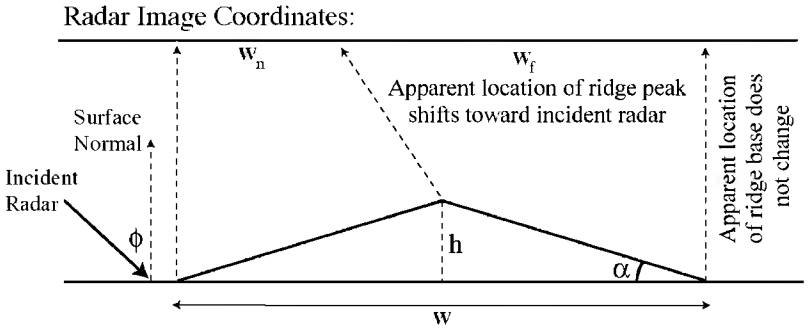

Figure 2. Sketch of geometry used to derive the ridge dimensions and scattering properties described in text. The ridge is assumed to have planar limbs, and the dashed line shows the radar image offset in ridge peak location due to the elevation difference between the peak and the plains. The near slope is foreshortened, and radar bright, while the far slope is elongated and radar dark. Abbreviations: w, belt width; w_n, width of slope facing the radar (near slope); w_f, width of far slope; h, ridge height; ϕ, nominal incidence angle; α, ridge slope angle.

first ratio represents a correction for scattering area, and the second represents the change in the diffuse echo due to the increased incidence angle.

[7] To compare the radar echo from the far slope of the ridge to the plains, we form a ratio,

$$T = \frac{\sigma^o_{R-corrected}}{\sigma^o_{plains}}. \quad (2)$$

If our assumptions above are correct, then a value of T close to unity implies that the far slope of the ridge has very similar morphology (at the decimeter scale relevant to 12.6-cm radar scattering) to the adjacent plains. This in turn suggests that the plains and the folded surface might be the same material unit, and thus the folding could postdate plains emplacement. If $T > 1$, the ridge slope is rougher than the plains. This may arise if the ridged terrain is comprised of an older, rougher unit, or if the ridge slope has been roughened by folding, or if the plains have been preferentially smoothed by fine-grained mantling material. Preferential smoothing of the plains without also smoothing the ridge surfaces is unlikely. The possibility that the ridge surfaces have been roughened by folding will be assessed below. If $T < 1$, the ridge slope is smoother than the plains, and thus the ridge almost certainly consists of older material (a younger, smoother material is highly unlikely because it would require emplacement of this material exactly atop the folded terrain).

4. Methods

[8] Ridges are characterized by bright, foreshortened slopes towards the radar (near slopes) and dark, elongated slopes away from the radar (far slopes). *Connors* [1995] published equations for determining the height and slope angles of surfaces sloping toward and away from the radar. For slopes away from the radar (far slopes),

$$w_f = h\left(\frac{1}{\tan\alpha} + \frac{1}{\tan\phi}\right). \quad (3)$$

For slopes toward the radar (near slopes),

$$w_n = h\left(\frac{1}{\tan\alpha} - \frac{1}{\tan\phi}\right), \quad (4)$$

where w_f is the width of the far slope on a SAR image, w_n = width of the near slope on a SAR image, h = height of slope, α = slope angle, and ϕ = the nominal incidence angle. These equations do not yield unique answers for isolated slopes. However, the near and far ridge slopes are connected at the crest of the ridge; that is, both slopes have the same value for h unless the ridge rests upon a significant transverse slope, an unlikely situation (see below). Because these ridges are generally inferred to be upright, low-amplitude folds, it also is reasonable to assume that the slope angles are the same or very nearly so. Thus the two equations may be solved simultaneously, yielding

$$h = \frac{\tan\phi}{2}\left(w_f - w_n\right) \quad (5)$$

$$\tan\alpha = \frac{2h}{w}, \quad (6)$$

where w is the total width of the belt. Widths are measured in the radar down-range direction. Depending on the geometry of the fold, and on the nominal incidence angle, the crest of the ridge will show a gradual change from bright to dark as one traverses the ridge in the radar down-range direction, or else an abrupt change in brightness. In some instances it can be difficult to determine the exact location of the ridge crest. If the down-range direction is not normal or close to normal to the trend of a ridge belt then the measured widths can be corrected using the cosine of the angle between the radar down-range direction and the normal to the trend of the ridge. This correction is necessary to obtain an accurate value for the ridge height, but is not necessary for slope angle because the cosine correction factor occurs in both the numerator and denominator of (6). These measurements are made on either FMIDR's or FMAPS at full 75 m/pixel resolution.

[9] Using a program developed by *Campbell* [1995], we derive the median backscatter coefficient of far ridge slopes for a number of ridges in each ridge belt to obtain multiple values for T, relative to the backscatter coefficient of a relatively large sample area in the nearby "regional" plains. The median value was chosen to avoid the strong biases introduced into a mean backscatter value by the occasional very bright pixel value. There generally is a good deal of scatter in these results, probably due to variations in the backscatter properties of the plains along the length of a ridge belt, true differences in the material making up the ridges in different parts of a ridge belt, or errors in determining ridge slope angle. The obvious variability of plains backscatter suggests that this is a major cause of scatter in T values. In many cases, the plains close to the ridge belt have different brightness values than those at some distance. We have thus also determined T values for the ridge slopes relative to these "adjacent" plains.

5. General Results

[10] The USGS web site (http://planetarynames.wr.usgs.gov/jsp/SystemSearch2.jsp ?System=Venus) contains 100 entries for the term "dorsum, pl. dorsa." Although many dorsa are ridge belts, more than half are not. Many are simply bundles of closely spaced wrinkle ridges or else long, narrow regions of contrasting backscatter with no associated ridge-like topography. Of those that are ridge belts, a few are not amenable to our methods because they trend ~NW, parallel to the radar look direction. Others are not suitable because they lack FMIDR coverage (C1-MIDRs generally do not permit backscatter sampling for areas large enough to include a significant number of far-slope pixels, and FMAPS have undergone some cosmetic adjustments that render them unreliable for quantitative studies such as this one). We found 10 ridge belts oriented at moderate to high angles to the radar look direction and for which there is sufficient FMIDR coverage. Two of these belts are not named, and thus are not included in the Flagstaff web site. Our results for all 10 belts are presented in Appendix A. Five belts of particular interest will be discussed in detail below.

[11] Overall, we observe that T values near or below unity occur primarily in the comparisons to adjacent plains; comparing the ridge far slopes to regional plains yields T

values that are generally >1 (Figure 3). On the basis of our discussions above, this suggests two major conclusions: (1) areas close to many ridges are preferentially higher in radar brightness than more distant plains, and (2) most ridge-forming terrain appears to be rougher, at the decimeter scale, than the regional plains. We interpret the first conclusion to indicate aeolian deposition of relatively rough (at centimeter scale) deposits adjacent to topographic obstacles, or to inherently brighter material associated with the ridge belt.

[12] Because the grain size of wind-transported materials is likely too small to affect centimeter-wavelength radar backscatter [*Greeley et al.*, 1997], it seems anomalous that aeolian deposits should be radar-bright. However, similar radar-bright deposits with wispy contacts have been noted elsewhere on Venus, and attributed to centimeter-scale aeolian microdunes or ripples [*Weitz et al.*, 1994].

[13] The second conclusion suggests one of three possible scenarios: (1) the ridge-forming terrain has been significantly roughened at the centimeter to decimeter scale by the folding process, (2) the ridges are folded plains, but we have introduced systematic biases into the estimation of "true" ridge terrain backscatter, or (3) the ridge-forming terrain preserves an older material unit that was roughened by weathering or tectonic processes prior to the development of the fold structures. We examine aspects of these scenarios below.

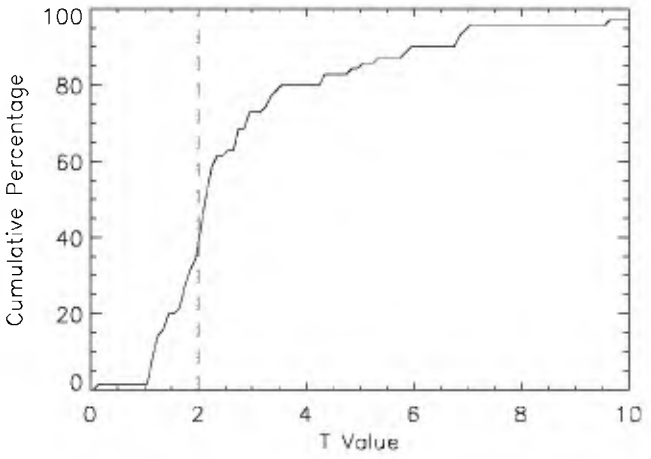

Figure 3. Cumulative percentage of model-derived T values for all ridge sample sites, relative to the regional plains. Values to the right of the dashed vertical line at $T = 2$ are confidently classified as "ridge-forming terrain rougher than the regional plains." Values of T between 1 and 2 may also indicate belt material that is rougher than regional plains material. Values of $T \sim 1$ indicate similarity of the ridge-forming and plains-forming materials.

6. Evaluating the Assumptions

6.1. Errors in Determining Slope Angle

[14] The uncertainty regarding the location of the ridge crest is a possible source of error in the determination of the slope angle. A nominal 1–2 pixel error in locating the crest of a ridge will create an error in α that is significant for gentle slopes but not for steeper slopes. Fortunately, a relatively large error in determining a gentle slope will not greatly affect the calculated T value, because the slope angle will still be small relative to the nominal incidence angle. Steeper slopes have more influence on T values, but are relatively little affected by 1–2 pixel errors in locating ridge crests, and thus the error carried forward to a calculated T value is not significant.

6.2. Assumption of Negligible Regional Slope

[15] A global map of surface slopes indicates that slopes on the flanks of ridge belts rarely exceed 2°; slopes over the center of ridge belts are even gentler, and thus the assumption of negligible regional slope seems justified for almost all sites. To evaluate the effect of steeper slopes, we tested the impact of regional tilts of up to 10° on the inferred slopes of ridges, and also on the resulting T values. For a ridge with slope of 8°, imaged at a nominal incidence angle of 35°, the area and scatter-law correction factors have a net value of 1.41. If the background terrain tilts away from the radar by 10°, the same degree of parallax offset in the peak of the ridge corresponds to an 11° ridge slope and a nominal 45° incidence angle. This leads to a net correction factor of 1.67. If the tilt is 10° toward the radar, then we have a 5° ridge slope and a 25° nominal incidence angle. This yields a net correction factor of 1.27. Overall, these observations suggest that the major result of the paper, that "T" values are consistently higher than unity, will not be greatly affected by regional slopes.

6.3. Form of the Diffuse Backscatter Law

[16] Rocky surfaces tend to have diffuse backscatter with a dependence on incidence angle given by $\cos^{-n} \phi$, where n ranges from about 1 to 2, depending upon the surface roughness. We have adopted a value of $n = 1.5$, but variations in this parameter for the actual surfaces could lead to some variation in the derived T values. In general, lower values of n lead to lower values of T, and higher values of n lead to higher values of T. The maximum range of these changes in T for $n = 1.5 \pm 0.5$ for large ridge angles, α, is ~60%, so we conservatively treat T values as "high" only when $T = 2$ or more. Values of T between 1 and 2 are regarded as "likely" to indicate a ridge surface that is rougher than regional plains. The cumulative histogram of values (Figure 3) shows that ~65% of all sampled ridge slope areas have $T > 2$ when ratioed to regional plains, and most of the remaining areas fall in the range between $T = 1$ and $T = 2$. Our general conclusions are thus not biased by the form of the diffuse backscatter function.

6.4. Form of the Equation for α

[17] The equation for determination of α implies that the ridge flanks are planar and the ridge has the shape of a very open, inverted V. However, folds generally have limbs that approximate sinusoidal rather than planar shapes. Assume a sinusoidal ridge shape. If the ridge extends from $-w/2$ to $+w/2$ on the x-axis, and has a height at the center of h, then the ridge shape is given by

$$z(x) = \frac{h}{2}\left[1 + \cos\left(\frac{2\pi x}{w}\right)\right] \tag{7}$$

and the slope (in radians) is

$$\alpha = \frac{dz}{dx} = -\frac{\pi h}{w}\sin\left(\frac{2\pi x}{w}\right), \quad (8)$$

where x and z are the horizontal and vertical coordinate axes, respectfully. Thus $z(x) = 0$ at $x = -w/2$ and $x = +w/2$. If a particular surface has a backscatter coefficient σ^o at the nominal incidence angle, ϕ, for a locally plane surface, then there are two effects that act to lower the backscatter of this surface when it forms the far slope of the ridge (Figure 2).

[18] The scattering area of a tilted facet is smaller than that used to normalize the radar map when the effective incidence angle is greater than the nominal value, ϕ. As a result, the far slope of the ridge appears darker than it would if there were no slope. The surface also appears darker because the backscattered return diminishes with incidence angle. Taken together, these effects lead to an approximately sinusoidal brightness profile over the far ridge limb. At the crest and base of the ridge, the backscatter is not affected by slope effects. At the center of the fold limb, the effective incidence angle is greatest, so the radar brightness reaches a minimum. The average brightness calculated by integrating over this sinusoidal ridge shape is very similar to that obtained by simply applying the two effects to a planar ridge flank (6). As the slope of the ridge increases, the difference in radar backscatter from base to center increases, but the error in using the planar assumption is still relatively low. In summary, the ridge slope shape has a relatively small impact on the average backscatter behavior of the far slope, so a good first-order result may be obtained by correcting the observed radar brightness by the area effect calculated for a planar ridge fold.

6.5. Evaluating Roughening of Plains Materials by Folding

[19] Assume a sinusoidal form for a ridge-belt ridge (7). The ridge profile is from $-w/2$ to $+w/2$, and $x = 0$ is at the ridge crest. The second derivative of this equation is the curvature, c, as a function of x,

$$\frac{d^2z}{dx^2} = -\left(\frac{2\pi^2 h}{w^2}\right)\cos\left[\frac{2\pi x}{w}\right] = c. \quad (9)$$

Fiber strain, ε, is $c * (t/2)$, where t is the thickness of the layer that is folded, and the fiber stress is $E^*\varepsilon$. For intact rock, E is Young's modulus; for bulk rock bodies, E is an appropriate deformation modulus that takes into consideration the universal presence of fractures and other flaws in large bodies of rock [*Schultz*, 1993]. *Schultz* [1993] estimates Young's modulus for basalt to be ~73 GPa. He estimates the bulk rock deformation modulus on Venus to be ~30–50 GPa. Tensile strength of intact basalt is estimated to be ~−14 MPa, and for bulk rock on Venus it is estimated to be ~−0.2 to −2 MPa.

[20] As an example, let us assume $w = 1000$ m and slope angle = 5°, yielding $h = 44$ m. For these values, $c = -0.000869$ m^{-1} at the crest of the ridge (x = 0). If we assume that the surface basalt layer is 1 m thick, then fiber strain, ε, at the ridge crest = −0.000435. Assuming a deformation modulus of 40 GPa (midrange from *Schultz* [1993]), the stress ($E^*\varepsilon$) at the ridge crest for these values would be ~−17 MPa. This is slightly greater (in a negative sense) than the tensile strength of intact rock, but it is an order of magnitude greater than the bulk rock tensile strength. Steeper slope angles and thicker folded layers will increase the magnitudes of strain and stress values. Thus the intact rock strength is not relevant because the rock will fail on preexisting fractures long before the stress reaches a value equal to the intact rock strength. The inference is that the rock would lengthen in a direction normal to the trend of the ridge by widening of favorably oriented preexisting fractures. Strain, and thus widening, will be greatest at the ridge crest, declining to zero at the inflection point of the sinusoidal curve. Below the inflection point the surface will be in compression, and no deformation would be expected.

[21] For our assumed ridge with 5° slopes, we can estimate the amount of widening that would likely occur. The integrated strain between the ridge crest and the inflection point (a distance of 250 m) is half that at the ridge crest. Thus total extension = 0.5 * 250 *.000435 = ~.05 m. If favorably oriented fractures are ~1 m apart (reasonable and conservative for basalt columnar joints), then each joint would open by ~0.2 mm. For a slope of 25°, the joints would open by about 1 mm for a 1-m-thick surface layer. If we also assume that the surface layer is 10 m thick (a large thickness for an assumed mechanically coherent layer), then the joints would open by about 1 cm. These small changes would be separated by a meter or so of unchanged rock. In that we are dealing with centimeter-scale radar, it is probable that the effect on backscatter of joint widening will be modest.

[22] An independent evaluation derives from the expectation that if surface roughening is caused by the folding, then this roughening should correlate with ridge slope angle; that is, the tighter the fold, the more likely that there would be surface roughening, either by fracturing or by mass wasting. On a plot of slope angle versus T value, most sites with slope angles less than about 22° fall in an elongated cluster parallel to the slope axis of the plot, indicating no correlation of slope angle and T. Thus the ridges in this elongated cluster appear to have been roughened primarily by some process other than widening of surface cracks during folding. For slopes greater than about 15° the scatter becomes much greater, and at high slope angles T tends to be very large. This may suggest a more important role for surface cracks and mass wasting once the ridge deformation reaches a particular level.

7. Results for Specific Fold Belts

7.1. Laūma Dorsa

[23] Laūma Dorsa is located in the western part of the Pandrosos Dorsa (V-5) quadrangle. It is part of the "ridge belt plains-fan assemblage" defined from Venera data [*Sukhanov et al.*, 1989; *Frank and Head*, 1990]. The belt is oriented north-south and is ~1,500 km long and 30–90 km wide. Laūma Dorsa differs from most ridge belts in being lower than surrounding plains rather than higher [*Rosenberg and McGill*, 2001]. The age of the ridges in this belt relative to regional plains is somewhat ambiguous. The belt ridges are mapped as deforming two of the three regional plains units (pr_a and pr_b) present in the Pandrosos

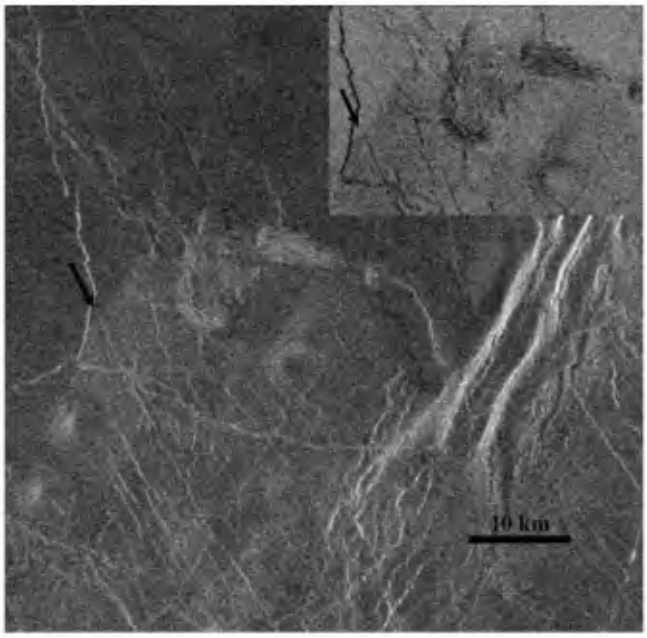

Figure 4. Contact between regional plains unit pr_c [*Rosenberg and McGill*, 2001] and belt materials of unit bl_a, Pandrosos Dorsa quadrangle. The plains materials are superposed on structures that cut the belt material, and thus the regional plains are younger than the material within Pandrosos Dorsa. Insert shows a portion of the contact zone in inverted format to highlight the structural features. Arrows point to corresponding points on the main image and the insert where a belt lineation is truncated by regional plains materials. North is up.

Dorsa quadrangle [*Rosenberg and McGill*, 2001], implying that Laūma Dorsa is younger than regional plains. However, it also is possible to interpret the relationship as one of embayment of the ridge belt by the regional plains (Figure 1).

[24] Relative to the regional plains, all of the derived T values for Laūma Dorsa are >1, although half lie between T values of 1 and 2. Many of these far-slope sites, however, have $T < 1$ when compared to the adjacent plains material. The former relationship suggests that the ridge slopes are rougher than the regional plains, and so are likely to be older material that predates plains emplacement. The latter relationship suggests just the opposite, but we infer that the "brighter" plains near the ridge belt have been modified by surficial (perhaps aeolian) materials.

[25] The basal contact of unit pr_a is transverse to the belt, a relationship suggesting that the ridges are younger than the plains. However, there is good evidence elsewhere in the region that long-wavelength warping is younger than the plains, suggesting that the transverse orientation of plains contacts here may date to before the current broad-scale topography was formed [*Rosenberg and McGill*, 2001]. Overall, the radar data favor ridges older than the plains, but this interpretation is less robust than for other belts.

7.2. Pandrosos Dorsa

[26] Pandrosos Dorsa is a very large ridge belt in the V-5 Quadrangle that consists of a complicated array of ridges and fractures that occur as "sub-belts" within the overall Dorsa [*Rosenberg and McGill*, 2001; *McGill*, 2003]. Pandrosos Dorsa also is part of the "ridge belt plains-fan assemblage." However, Magellan data demonstrate that Pandrosos Dorsa consists of both contractional and extensional structures that are in many places about parallel to each other [*Rosenberg and McGill*, 2001].

[27] Most of Pandrosos Dorsa trends N-S and is centered on longitude 205°E. The south end of the belt is at ~52°N, the north end at ~67°N. At ~58°N the belt splits into a narrow northern continuation of Pandrosos Dorsa to the east and Anpao Dorsa to the west. The total length of Pandrosos Dorsa is ~1600 km, and its width varies from 60 km in the north to 230 km in the south. Most of the ridges occur in assemblages that are oriented about parallel to the overall trend of the belt, and which generally are separated from each other by zones of intense development of extensional structures, many of which are grabens. The ridge assemblages range in length from 150 to 1000 km, and in width from 25 to 75 km.

[28] Pandrosos Dorsa is bounded on the west by two of the three mapped regional plains material units (pr_a and pr_c) [*Rosenberg and McGill*, 2001]. At ~58°N the western margin of the belt steps eastward, providing a transverse contact between regional plains and the belt. At this step there is a clear contact between regional plains (pr_c) and the material (bl_a) making up the belt where this belt material is less deformed into ridges and fractures than is generally the case. The structures that are present on the belt material are sharply truncated at the contact with regional plains (Figure 4). Geologic evidence from the radar image data thus strongly suggests that the materials forming Pandrosos Dorsa were emplaced, and most of the deformation accomplished, prior to the emplacement of the surrounding plains.

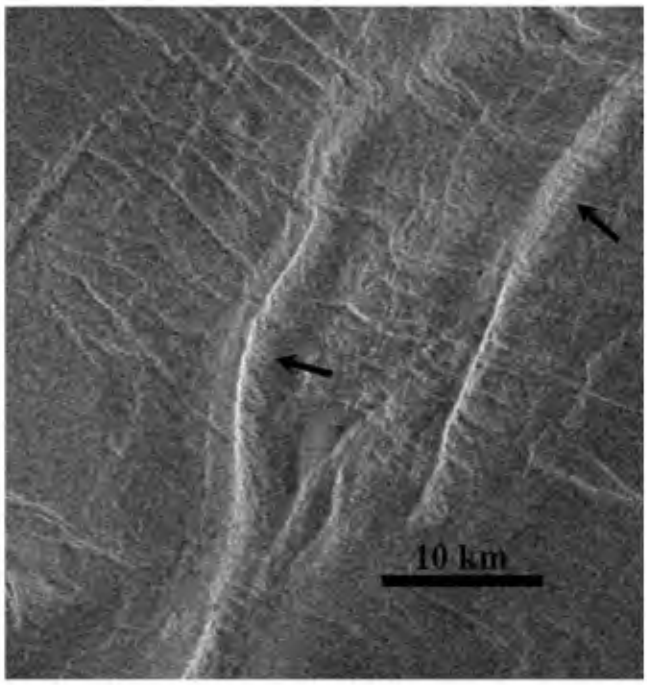

Figure 5. Lineations cutting ridge belt ridges truncated (arrows) at contacts with surrounding regional plains, Lavinia Planitia quadrangle. North is up.

Figure 6. Radar-bright materials bounding both sides of Vedma Dorsa inferred to be a thin aeolian blanket deposited owing to interference with the wind by the belt ridges. Note suggestion at bottom center that this bright material is dammed by a wrinkle ridge. It also has indistinct contacts with surrounding regional plains. Belt is in the Nemesis Tessera quadrangle. North is up.

[29] The eastern margin of Pandrosos Dorsa is bounded by large flow fields (unit fd) from its southern end northward to ~58°N. These flows clearly truncate extensional structures in the belt, and appear to embay belt ridges as well. However, some belt extensional structures cut the flows, and because these flow fields are superposed on regional plains [*Rosenberg and McGill*, 2001], this relationship demonstrates that some of the belt extensional structures are younger than regional plains, and thus that the extensional deformation was progressive.

[30] Radar data were collected at nine sites within southern Pandrosos Dorsa. Five of these sampled plains-like materials that are from within the belt (Appendix A), and these yield T values (0.98, 0.82, 1.04, 1.32, 1.22) that, within our bounds of confidence, are consistent with Pandrosos ridges having formed by folding plains-like belt materials, in agreement with the geological evidence. Two of the sites (7 and 9) compare ridge slopes to materials outside of the belt. The exterior material at site 7 is part of a large fluctus unit (fd) that embays and truncates belt structures [*Rosenberg and McGill*, 2001]. The T value of 2.12 is not consistent with the ridge folding fluctus material, also in agreement with the geologic evidence. Site 9 involves materials of two map units outside of the belt [*Rosenberg and McGill*, 2001]; a radar-dark (pr_c) unit immediately adjacent to the ridge belt (T = 2.22), and a younger, brighter unit (pr_a) not in contact with the ridge belt (T = 1.46). We again interpret these data to mean that the ridge-forming material is rougher than the nearby terrain, and thus likely did not form by folding the regional plains materials.

7.3. Unnamed Belt in Lavinia Planitia

[31] In the northeast part of the Lavinia Planitia Quadrangle (V-55) is a small northeast-trending ridge belt mapped as older than the regional plains [*Ivanov and Head*, 2001]. Both the plains around this belt and the ridges within the belt are cut by northwest-trending fractures and grabens associated with Antiope Linea. In addition, the ridges of the belt are characterized by generally narrow fractures that are confined to the ridge material (unit prg); that is, these narrow fractures are truncated at contacts with the surrounding plains of unit pwr_1 (Figure 5). This provides robust evidence that the ridge belt is older than the surrounding plains.

[32] Of the three radar-data sites, two have $T > 2$, favoring an age of ridge material older than regional

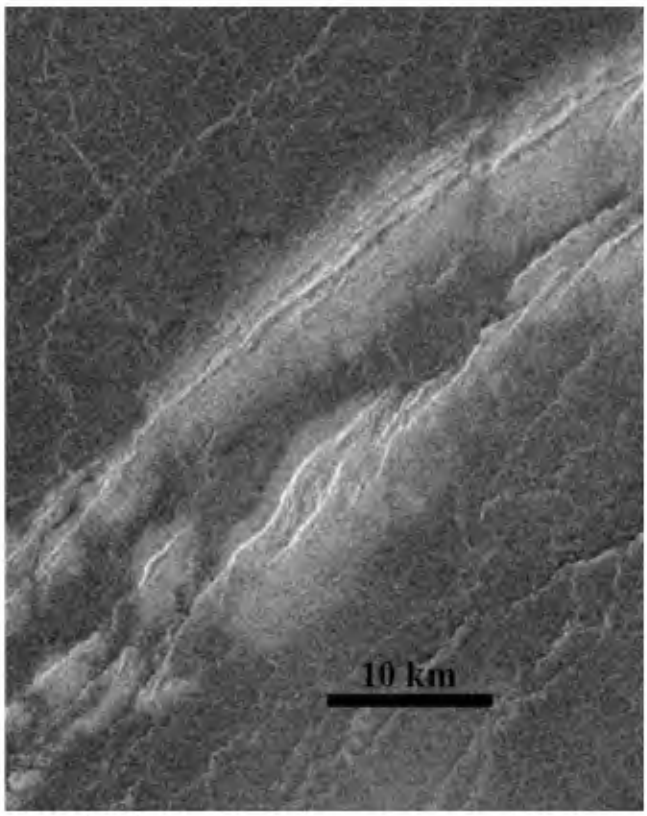

Figure 7. Patchy radar-bright material associated with Mardezh-Ava Dorsa, Tellus Tessera quadrangle. Note wispy contacts with surrounding regional plains, suggesting an aeolian origin for the bright material. North is up.

plains, in agreement with the geological observations. Site 1 yields a T value close to 1, but the material adjacent to the ridge appears brighter and more fractured than nearby regional plains. Our interpretation is that site 1 includes a plains-like material that is older than the local regional plains, in agreement with *Ivanov and Head* [2001].

7.4. Vedma Dorsa

[33] Vedma Dorsa is located in the western part of the Nemesis Tessera (V-13) quadrangle. It is oriented approximately north-south from 27°N, 157°E to 55°N, 170°E, a distance of ~3000 km. Age relationships with neighboring plains materials are complex. Radar data were collected at 17 sites. In places there is a relatively bright material immediately adjacent to the ridge belt. Locally this material has wispy contacts with adjacent regional plains materials (Figure 6), and is probably surficial (possibly aeolian). This wispy material is present at sites 1–4 and 16–17. At sites 6, 7, and 13 the adjacent relatively bright material is a mappable unit that is older than the regional plains, on the basis of evidence that the plains materials truncate structures that deform the radar bright material.

[34] Adjacent plains at sites 1–4 are the wispy surficial material, and thus the T values almost certainly carry no stratigraphic meaning. The wispy material at sites 16 and 17 was not sampled. All but one of the T values involving regional plains are >1, and thus we infer that the ridges of Vedma Dorsa do not consist of folded regional plains.

7.5. Frigg Dorsa

[35] Frigg Dorsa is mostly within the Velamo Planitia (V-12) quadrangle, but also extends into the Nemesis Tessera (V-13) and Atalanta Planitia (V-4) quadrangles. As is the case for Vedma Dorsa, the plains around the belt display significant variations in backscatter, with plains close to the belt commonly characterized by higher backscatter than more distal plains. This results in two sites yielding T values with respect to adjacent plains of ~1. However, most adjacent plains and all regional plains in the vicinity of Frigg Dorsa yield $T > 1$, with regional plains at site 2 a possible exception. The consistent high T values supports the implication that the ridges of this belt did not form by folding regional plains.

8. Discussion and Conclusions

[36] Despite the scatter in T values, it is possible to draw some interesting and useful conclusions from the results of this study. Several of the ridge belts studied are directly bordered by a relatively radar-bright, homogeneous material that commonly is characterized by wispy contacts with regional plains (Figure 7). This results in T values for adjacent plains that are lower than those determined with respect to the regional plains. However, it is likely that this bright homogeneous material was deposited by aeolian processes or, less likely, is due to mass wasting off the ridge-belt ridges. Presumably, the positive topography of ridge belts interfered with wind patterns sufficiently to cause deposition of aeolian blankets next to the belts. Thus the relatively high backscatter of many adjacent plains sites would be due to deposits that are younger than the ridge belts (and the materials of the belts), and thus the T values calculated tell us nothing about materials forming the ridges.

[37] With few exceptions, the T values for ridge far slopes relative to the regional plains are >1, implying that the ridge surface is rougher at the decimeter scale than the plains. Our model for ridge formation above suggests that there is no significant change in the small-scale roughness from such gentle folding, and thus we infer that the ridges formed in materials that predate the plains and that were rougher than the plains prior to folding. This greater roughness could be due to an older plains surface having been subjected to more episodes of fracturing than would a younger surface. Weathering may play a role as well. There is evidence that rough surfaces on Venus are smoothed by weathering [*Arvidson et al.*, 1992], and that originally smooth surfaces can be roughened by weathering (such as the gradual fragmenting of smooth glass coatings on pahoehoe flows noted by *Campbell and Shepard* [1996]). Older surfaces logically would have weathered more than younger surfaces.

[38] Assuming that our sample of ridge belts is representative, the results of our radar studies and independent geologic evidence for some belts lead us to conclude that the material forming ridge belts is dominantly older than that forming the regional plains. What this means on a global scale is uncertain; without a statistically significant crater-timescale [*Campbell*, 1999] or other tool for dating, we cannot determine if all ridge belts (or all regional plains) are coeval. On a regional scale, however, there appears to be a "directional" behavior in the development of ridge belts and plains materials across Venus.

Appendix A

[39] Data Tables A1–A10 follow for each of the 10 sampled ridge belts. Some individual sites are annotated for clarity. All backscatter values are medians.

[40] From left to right, the columns are: site number, latitude, longitude, nominal incidence angle (ϕ), ridge slope angle (α), backscatter of ridge far slope, backscatter of plains adjacent to the ridge, backscatter of regional plains, T calculated for scatter of ridge far slope and adjacent plains, T calculated for scatter of ridge far slope and regional plains.

[41] Latitude and longitude of each numbered site refer to the ridge. The backscatter for the far limb is sampled within a rectangular area that is confined to the far limb. Related plains backscatter may be sampled immediately adjacent to the ridge far limb (adjacent plains) or at some greater distance (regional plains). For some sites adjacent and regional plains are identical, as is apparent from the repeated numbers in the data tables.

[42] In several places the adjacent plains consist of an area of relatively bright material along one or both side of a ridge belt. Commonly, this material has poorly defined or "wispy" contacts, and locally it appears to be ponded by wrinkle ridges. Because this material is relatively bright, the T values tend to be ~1 or smaller. Most likely, this material is an aeolian blanket that has been deposited where it is as a result of the ridges of the ridge belt interfering with wind patterns. Locally, it is possible that this material is due to mass wasting from the belt ridges. We infer that the T values calculated for this material provide no useful stratigraphic information.

Table A1. Frigg Dorsa

Site Number	Lat.	Lon.	ϕ	α	σo far	σo Padj	σo Preg	Tadj	Treg
1	51.38	150.70	32.13	14.5	0.0182	0.0459	0.0152	0.74	2.24
2	51.24	150.60	32.20	11.8	0.0152	0.0208	0.0208	1.22	1.22
3	51.23	150.58	32.21	15.8	0.0239	0.0208	0.0208	2.28	2.28
4	50.83	150.43	32.42	20.8	0.0170	0.0246	0.0246	1.73	1.73
5	50.79	150.39	32.44	21.9	0.0258		0.0246		2.77
6	50.09	149.76	32.81	9.5	0.0199	0.0288	0.0151	1.04	1.98
7	50.25	150.19	32.72	17.3	0.0241	0.0240	0.0240	2.13	2.13
8	49.57	149.96	33.08	21.3	0.0204	0.0491	0.0194	1.07	2.70
9	49.52	149.93	33.11	21.7	0.0245	0.0491	0.0194	1.31	3.31
10	49.37	149.89	33.19	14.4	0.0369	0.0491	0.0194	1.40	3.54
11	48.93	149.83	33.42	16.7	0.0302		0.0209		2.99
12	48.37	149.50	33.71	22.5	0.0295		0.0118		6.85
13	48.29	149.41	33.75	16.0	0.0194		0.0118		3.30
14	48.28	149.48	33.76	13.7	0.0388	0.0467	0.0118	1.50	5.94
15	48.07	149.47	33.87	15.0	0.0423		0.0161		5.04

Table A2. Unnamed Dorsa, Ganiki Planitia

Site Number	Lat.	Lon.	ϕ	α	σo far	σo Padj	σo Preg	Tadj	Treg
1	46.39	209.27	34.71	20.2	0.0501	0.0576	0.0378	2.14	3.26
2	46.19	209.14	34.81	19.2	0.0344	0.1582	0.0378	0.51	2.13
3	45.68	208.41	35.06	5.2	0.0588	0.0646	0.0341	1.14	2.16
4	45.98	208.39	34.91	11.2	0.0715	0.3445	0.0341	0.34	3.40
5	45.46	209.14	35.17	7.1	0.0221	0.0278	0.0243	1.08	1.23
6	44.92	209.13	35.44	12.6	0.0239	0.0287	0.0239	1.44	1.72
7	45.12	208.84	35.34	7.5	0.0363	0.0479	0.0239	1.05	2.09

Table A3. Hemera Dorsa

Site Number	Lat.	Lon.	ϕ	α	σo far	σo Padj	σo Preg	Tadj	Treg
1	51.52	243.31	32.05	15.0	0.0350		0.0305		2.20
2	49.98	243.59	32.87	19.3	0.0499		0.0217		5.36
3	47.67	244.18	34.07	19.4	0.0288		0.0288		2.35

Table A4. Laūma Dorsa[a]

Site Number	Lat.	Lon.	ϕ	α	σo far	σo Padj	σo Preg	Tadj	Treg
1	67.15	191.24	24.98	10.0	0.0664		0.0837		1.25
2	66.40	187.53	25.26	13.3	0.0589		0.0615		1.72
3	66.70	190.28	25.15	12.0	0.1086		0.1306		1.43
4	65.87	187.31	25.47	6.3	0.0605	0.0664	0.0732	1.22	1.11
5	65.04	185.52	25.80	13.6	0.0740		0.0706		1.92
6	65.33	185.67	25.69	7.4	0.0566		0.0566		1.40
7	65.24	192.31	25.72	10.2	0.1030	0.2983	0.0780	0.55	2.09
8	65.26	191.97	25.72	4.6	0.1880	0.2720	0.0780	0.86	2.99
9	65.13	192.02	25.77	9.1	0.1180	0.2147	0.0780	0.83	2.29
11	63.73	189.32	26.33	5.0	0.0811	0.3097E		0.33	
11						0.1227W		0.83	
12	63.86	191.51	26.28	8.7	0.1556	0.2250	0.0851	1.03	2.71
13	63.59	191.82	26.39	7.7	0.1280	0.2250	0.0851	0.81	2.13
14	62.76	190.04	26.74	1.9	0.1564	0.0781		2.19	

[a]Laūma Dorsa site 11 sampled adjacent plains twice; east of the ridge (E) and west of the ridge (W). Adjacent plains for sites 12 and 13 have wispy contacts with regional plains. Regional plains not sampled at site 11 because they contain pervasive, bright cellular structures that would artificially elevate the radar return from a sample box.

Table A5. Unnamed Dorsa, Lavinia Planitia[a]

Site Number	Lat.	Lon.	ϕ	α	σo far	σo Padj	σo Preg	Tadj	Treg
1	−37.85	348.31	28.54	10.7	0.0807		0.1171		1.10
2	−38.24	348.07	28.35	11.3	0.0782		0.0622		2.06
3	−41.78	349.43	26.65	4.1	0.0865		0.0495		2.11

[a]The ridge at site 1 is cut by fine-scale lineaments that are abruptly truncated at contacts with regional plains. The regional plains at this site are brighter than at most sites, consistent with the calculated T value of 1.1. For this site the geological evidence that the ridge material is older than the plains material is robust, so we must infer that the 1.1 T value means that the older material making up that ridge has radar properties approximately the same as plains materials.

Table A6. Mardezh-Ava Dorsa[a]

Site Number	Lat.	Lon.	ϕ	α	σo far	σo Padj	σo Preg	Tadj	Treg
1	32.38	68.74	41.19	16.3	0.0783	0.0820	0.0094	2.02	17.67
2	31.20	67.25	41.63	25.4	0.0316	0.0459	0.0138	1.47	4.88
3	31.33	67.32	41.59	33.7	0.0317		0.0139		16.80
4	30.19	66.00	42.03	29.4	0.0269		0.0141		9.62

[a]Adjacent plains at site 1 have wispy contacts with regional plains. Adjacent plains at site 4 appear to be a mappable unit that is cut by closely spaced bright lineations. The lineations preclude calculating a meaningful T value.

Table A7. Pandrosos Dorsa[a]

Site Number	Lat.	Lon.	ϕ	α	σo far	σo Padj	σo Preg	Tadj	Treg
1	52.70	208.33	31.45	5.8	0.0669	0.1468		0.59	
2	53.13	206.38	31.24	11.4	0.0746	0.1240		0.98	
3	53.20	208.43	31.20	4.1	0.0517	0.1245		0.50	
4	53.70	207.08	30.95	6.0	0.0664	0.1053		0.82	
5	54.47	206.08	30.57	7.4	0.0717	0.0950		1.04	
6	56.65	206.68	29.47	13.2	0.0593	0.1081		0.97	
7	57.28	209.09	29.18	17.2	0.0580		0.0579		2.12
8	58.48	208.72	28.65	9.4	0.0695	0.0799		1.32	
9	59.49	209.92	28.22	14.0	0.0572	0.0868	0.0475	1.22	2.22
9							0.0720		1.46

[a]"Adjacent plains" at sites 1–6, 8 and 9 are within the belt; site 1 sampled belt-interior bright flows, sites 2, 4, 5, 8 and 9 sampled plains-like materials, and sites 3 and 6 sampled "ponded," presumably volcanic, material within the belt. Site 7 involves fluctus material superposed on regional plains east of the belt. Site 9 includes two mapped regional plains units west of the belt (pr_a and pr_c of *Rosenberg and McGill* [2001]), the darker and older of which (pr_c) is immediately adjacent to the belt.

Table A8. Poludnitsa Dorsa[a]

Site Number	Lat.	Lon.	ϕ	α	σo far	σo Padj	σo Preg	Tadj	Treg
1	6.33	180.00	45.97	14.1	0.0353	0.0976	0.0370	0.72	1.89
2	5.84	180.06	45.94	7.2	0.0489	0.1233	0.0617	0.55	1.10
3	4.88	179.43	45.84	24.0	0.0356		0.0310		4.32
4	3.00	178.69	45.62	29.5	0.0238		0.0207		6.99

[a]Adjacent plains for sites 1 and 2 are plains-like materials within the ridge belt. The low T values may be due to increased backscatter of belt materials caused by abundant radar-bright lineations. Belt materials are embayed by regional plains.

Table A9. Saule Dorsa

Site Number	Lat.	Lon.	ϕ	α	σo far	σo Padj	σo Preg	Tadj	Treg
1	−57.63	205.95	21.21	6.2	0.0578		0.0579		1.37
2	−57.76	205.88	21.18	8.4	0.0766		0.0579		2.01
3	−59.52	204.53	20.80	5.7	0.1454		0.0915		2.14
4	−59.80	204.38	20.74	10.0	0.0440		0.0637		1.13
5	−62.09	204.48	20.30	12.5	0.0668		0.0668		1.84
6	−62.12	204.36	20.29	10.8	0.0638		0.0882		1.23
7	−62.19	204.12	20.28	10.0	0.0843		0.0805		1.72

Table A10. Vedma Dorsa[a]

Site Number	Lat.	Lon.	ϕ	α	σo far	σo Padj	σo Preg	Tadj	Treg
1	28.47	159.31	42.63	22.2	0.0205	0.0411	0.0283	1.54	2.35
2	28.31	159.31	42.69	28.3	0.0411	0.0410	0.0283	4.73	6.86
3	28.69	159.45	42.56	22.2	0.0343	0.0719	0.0238	1.45	4.37
4	28.80	159.56	42.52	17.0	0.0314	0.0689	0.0238	1.02	2.95
5	29.13	159.76	42.41	10.3	0.0302	0.0873	0.0228 E	0.55	2.10
5							0.0435 S		1.10
6	34.67	157.14	40.28	10.3	0.0499	0.2890	0.0314	0.27	2.50
7	34.66	157.17	40.28	13.0	0.0476	0.1146	0.0314	0.74	2.71
8	36.17	158.30	39.57	11.1	0.0249	0.2293	0.2293	0.18	0.18
9	37.12	157.40	39.14	11.5	0.0338	0.0338	0.0338	1.66	1.66
10	38.94	157.48	38.36	13.8	0.0257	0.0373		1.27	
11	39.32	157.87	38.18	18.6	0.0996	0.0327	0.0327	7.08	7.08
12	39.01	156.90	38.33	19.1	0.0310	0.0392	0.0392	1.89	1.89
13	40.84	155.57	37.43	16.4	0.0435	0.0724		1.25	
14	41.28	158.48	37.21	17.6	0.0724	0.0441	0.0231	3.60	6.88
15	38.95	158.45	38.35	9.7	0.0310	0.0235	0.0235	2.01	2.01
16	41.93	159.58	36.89	14.0	0.0342	0.0271	0.0271	2.33	2.33
17	42.07	159.54	36.82	22.2	0.0497	0.0237	0.0237	5.82	5.82

[a]Site 5 includes two regional plains localities, one east of the ridge (E), one south of the ridge (S). Adjacent plains have wispy contacts at sites 1–4 and 10. The regional plains embay the adjacent plains at sites 6 and 7. Regional plains at site 13 are mottled and streaked with bright lineaments and thus not sampled.

[43] **Acknowledgments.** This research was supported by NASA Planetary Geology and Geophysics grants NNG05G132G and NNG06GG73G to the University of Massachusetts, G. E. McGill, PI.D. Nunes and E. Stofan provided very useful and constructive reviews of our original draft.

References

Arvidson, R. E., et al. (1992), Surface modification of Venus as inferred from Magellan observations of plains, *J. Geophys. Res.*, *97*, 13,303–13,317.

Basilevsky, A. T., and J. W. Head III (1995), Global stratigraphy of Venus: Analysis of a random sample of thirty-six test areas, *Earth Moon Planets*, *66*, 285–336.

Basilevsky, A. T., and J. W. Head III (1998), The geologic history of Venus: A stratigraphic view, *J. Geophys. Res.*, *103*, 8531–9544.

Basilevsky, A. T., and J. W. Head (2000), Geologic units on Venus: Evidence for their global correlation, *Planet. Space Sci.*, *48*, 75–111.

Campbell, B. A. (1995), Use and presentation of Magellan quantitative data in Venus mapping, *U. S. Geol. Surv. Open File Rep.*, *95-519*.

Campbell, B. A. (1999), Surface formation rates and impact crater densities on Venus, *J. Geophys. Res.*, *104*, 21,951–21,955.

Campbell, B. A., and M. K. Shepard (1996), Lava flow surface roughness and depolarized radar scattering, *J. Geophys. Res.*, *101*, 18,941–18,952.

Connors, C. (1995), Determining heights and slopes of fault scarps and other surfaces on Venus using Magellan radar, *J. Geophys. Res.*, *100*, 14,361–14,382.

Frank, S. L., and J. W. Head (1990), Ridge belts on Venus: Morphology and origin, *Earth Moon Planets*, *50/51*, 421–470.

Greeley, R., K. C. Bender, R. S. Saunders, G. Schubert, and C. M. Weitz (1997), Aeolian processes and features on Venus, in *Venus II: Geology, Geophysics, Atmosphere, and Solar Wind Environment*, edited by S. W. Bougher, D. M. Hunten, and R. J. Phillips, pp. 547–589, Univ. of Ariz. Press, Tucson.

Guest, J. E., and E. R. Stofan (1999), A new view of the stratigraphic history of Venus, *Icarus*, *139*, 55–66.

Hagfors, T. (1970), Remote probing of the Moon by infrared and microwave emissions and radar, *Radio Sci.*, *5*, 189–227.

Ivanov, M. A., and J. W. Head III (2001), Geologic map of the Lavinia Planitia Quadrangle (V-55), Venus, *U.S. Geol. Surv. Invest. Ser. Map*, *I-2684*.

McGill, G. E. (2003), Kinematics of a linear deformation belt: The evolution of Pandrosos Dorsa, Venus, *Lunar Planet. Sci.*, *XXXIV*, abstract 1012.

Rosenberg, E., and G. E. McGill (2001), Geologic map of the Pandrosos Dorsa Quadrangle (V-5), Venus, *U.S. Geol. Surv. Invest. Ser. Map*, *I-2721*.

Schultz, R. A. (1993), Brittle strength of basaltic rock masses with applications to Venus, *J. Geophys. Res.*, *98*, 10,883–10,895.

Squyres, S. W., D. G. Jankowski, M. Simons, S. C. Solomon, B. H. Hager, and G. E. McGill (1992), Plains tectonism on Venus: The deformation belts of Lavinia Planitia, *J. Geophys. Res.*, *97*, 13,579–13,599.

Sukhanov, A. L., et al. (1989), Geomorphic/geologic map of part of the northern hemisphere of Venus, *U. S. Geol. Surv. Misc. Invest. Ser. Map*, *I-2059*.

Weitz, C. M., J. J. Plaut, R. Greeley, and R. S. Saunders (1994), Dunes and microdunes on Venus: Why were so few found in the Magellan data?, *Icarus*, *112*, 282–295.

B. A. Campbell, Center for Earth and Planetary Studies, Smithsonian Institution, PO Box 37012, Washington, DC 20013-7012, USA.

G. E. McGill, Department of Geosciences, University of Massachusetts, Morrill Science Center, 611 North Pleasant Street, Amherst, MA 01003, USA. (gmcgill@geo.umass.edu)